2018 European Control Conference (ECC)
June 12-15, 2018. Limassol, Cyprus

Sliding Mode Control Design for a Multidimensional Morphing UAV

Jihoon Lee[1], Seong-hun Kim[1], Seungyun Jung[1], Hanna Lee[1], and Youdan Kim[2]

Abstract— **In this study, a sliding mode controller is designed for a longitudinal dynamic model of a span and sweep-varying morphing unmanned aerial vehicle. Changes in aerodynamic and dynamic characteristics of the morphing wing aircraft model are investigated. Controller is designed based on an input-output linearization scheme to accomplish regulation and command tracking of airspeed and altitude. Numerical simulation is performed, and the results show that nominal tracking performance of the proposed controller is maintained even in the presence of the morphing wing configuration changes.**

I. INTRODUCTION

Historically, morphing aircraft has been introduced and studied to exploit the benefits of the morphing concepts [1]. In general, performance of morphing aircraft can be considerably improved by changing the external shape of the wing and/or fuselage during the flight. For example, enhanced tracking performance, expanded flight envelope, and increased mission adaptability can be achieved. On the other hand, it is difficult to design a control system for morphing aircraft because the dynamic characteristics are significantly affected by the configuration changes. Therefore, most of existing control methods for morphing aircraft use a robust control scheme, an adaptive control scheme, or a learning technique to account for the configuration changes [2].

In this study, a longitudinal dynamic model of a morphing unmanned aerial vehicle (UAV) is considered, and the dynamic characteristics in various span and sweep configurations are investigated. A sliding mode controller (SMC) is designed to accomplish airspeed and altitude tracking in various wing configurations. Note that our aim is to design a single controller that encompasses a wide range of configurations rather than to fit the UAV into a specific mission. Numerical simulation is performed to demonstrate the effectiveness of the proposed scheme, and the results imply that the transient and steady-state properties can be significantly improved by adjusting the wing configuration.

*This work was supported by the R&D Program in Aerospace Parts and Materials (10066055) through the Korea Evaluation Institute of Industrial Technology (KEIT) funded by the Ministry of Trade, Industry, and Energy (MOTIE), The Republic of Korea.

[1]J. Lee, S. Kim, S. Jung, and H. Lee are with the Department of Aerospace Engineering, Seoul National University, Seoul 08826, The Republic of Korea leejihoon@snu.ac.kr, bgbgof@snu.ac.kr, airwalk31@snu.ac.kr, hn_lee@snu.ac.kr

[2]Y. Kim is with Faculty of Aerospace Engineering, Institute of Advanced Aerospace Technology, Seoul National University, Seoul 08826, The Republic of Korea ydkim@snu.ac.kr

II. MORPHING UAV MODEL

In this section, a longitudinal dynamic model of a morphing UAV is explained.

A. Modeling

A morphing UAV is modeled to be capable of adjusting its span (from 3m to 4.446m) and sweep-back angle (from 0° to 40°) of the main wing. A span variation refers to changes in length of the main wing, and it is independent of a sweep-back angle. The center of mass and the moment of inertia are obtained by computer-aided design (CAD) modeling as shown in Fig. 1.

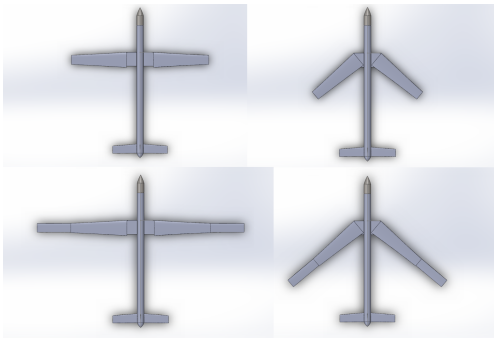

Fig. 1. Multidimensional morphing UAV CAD model: nominal (upper left), max span (lower left), max sweep (upper right), max span & sweep (lower right)

Lift, drag, and pitching moment coefficients corresponding to each configuration are obtained by using XFLR5 (Fig. 2); an analysis tool for airfoils, wings and planes operating at low Reynolds numbers based on the lifiting line theory, the vortex lattice method, and the 3D panel method [3]. Dimensionless coefficients are normalized by using the wing reference area $S = 0.84\text{m}^2$, length $\bar{c} = 0.288\text{m}$, and dynamic pressure in a cruise condition, i.e., $h = 300\text{m}$ and $V = 20\text{m/s}$.

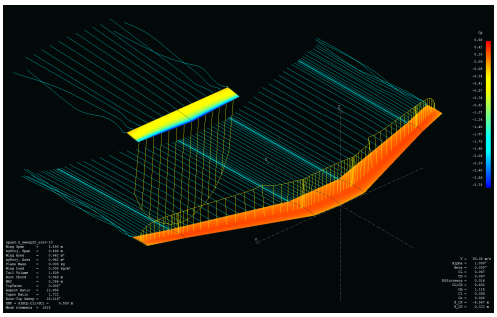

Fig. 2. XFLR5 Model

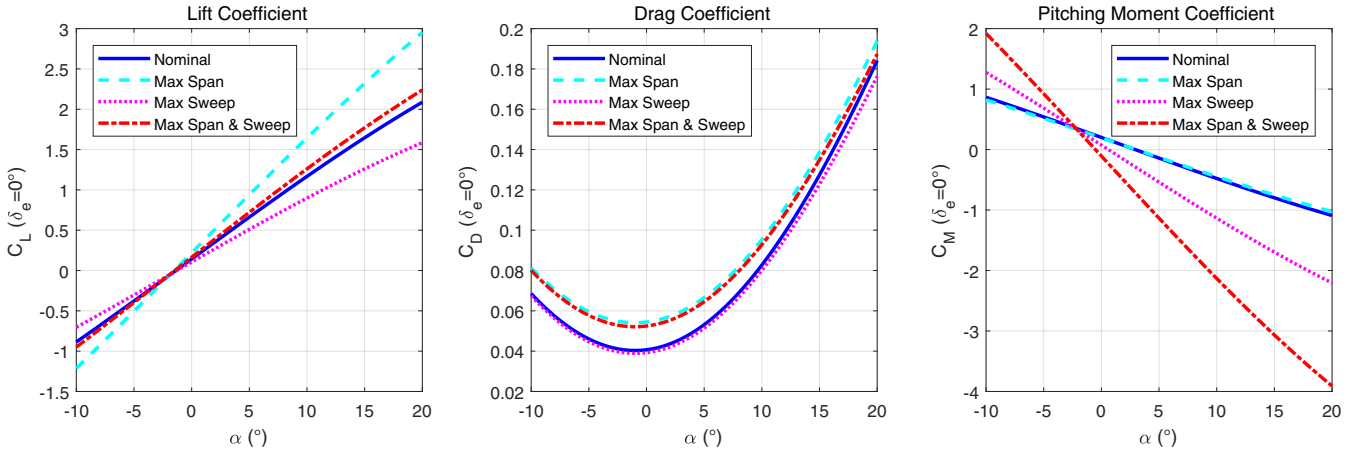

Fig. 3. Aerodynamic coefficients in four configurations

Aerodynamic coefficients of four different configurations are shown in Fig. 3. Note that sweeping-back makes a slope of the pitching moment steeper, which is mainly attributed to a backward shift of the center of pressure. Although span extension alone does not affect the slope of the pitching moment, significant changes are observed when it is combined with sweep-back angle change. It is also observed in the data that span extension tends to increase both lift and drag, but sweeping-back has the opposite effects. Figure 4 shows that the lift-to-drag ratio can be adjusted considering the operational purposes by changing the configuration.

B. Dynamics

The longitudinal dynamics of aircraft can be described as follows [4]

$$\dot{V} = \frac{T\cos\alpha - D}{m} - g\sin\gamma \tag{1}$$

$$\dot{\gamma} = \frac{L + T\sin\alpha}{mV} - \frac{g\cos\gamma}{V} \tag{2}$$

$$\dot{h} = V\sin\gamma \tag{3}$$

$$\dot{\alpha} = q - \dot{\gamma} \tag{4}$$

$$\dot{q} = \frac{M_y}{I_y} \tag{5}$$

where V, γ, h, α, q are true airspeed (TAS), flight path angle, altitude, angle of attack and pitch rate, respectively, and L, D, M_y, T, I_y, g are lift, drag, pitching moment, thrust, pitch-axis moment of inertia and the standard gravitational acceleration, respectively. Thrust is assumed to be aligned with the body X axis, and lift, drag, pitching moment and thrust are defined as follows

$$L = \tfrac{1}{2}\rho V^2 S C_L \tag{6}$$

$$D = \tfrac{1}{2}\rho V^2 S C_D \tag{7}$$

$$M_y = \tfrac{1}{2}\rho V^2 S\bar{c} C_M \tag{8}$$

$$T = T_{max}\sigma \tag{9}$$

where T_{max} is the maximum thrust. In this study, it is assumed that C_L, C_D, and C_M are dependent on the angle of attack $-10^\circ \le \alpha \le 20^\circ$, the elevator deflection $-10^\circ \le \delta_e \le 10^\circ$, the span extension ratio $0 \le \eta_1 \le 1$, and the sweep-back ratio $0 \le \eta_2 \le 1$. The engine model is assumed to follow the second order dynamics with saturation (10), and it is controlled by the throttle command σ_c.

$$\ddot{\sigma} + 2\zeta\omega_n\dot{\sigma} + \omega_n^2\sigma = \omega_n^2\sigma_c, \quad 0 \le \sigma \le 1 \tag{10}$$

where ζ and ω_n are the damping ratio and the undamped natural frequency, respectively. The engine parameters are set to common values for this class of UAV.

Considering the thrust and elevator deflection limits, a maximum and minimum value of true airspeed in a straight and level flight condition can be obtained by performing a trim analysis. Figure 5 shows that the minimum possible speed can be further decreased by extending the wing span, and the maximum speed can be further increased by sweeping-back. These results are due to the improved lift-to-drag ratio at the maximum span and the reduced drag in the maximum sweep-back. Open-loop poles are shown in Fig. 6.

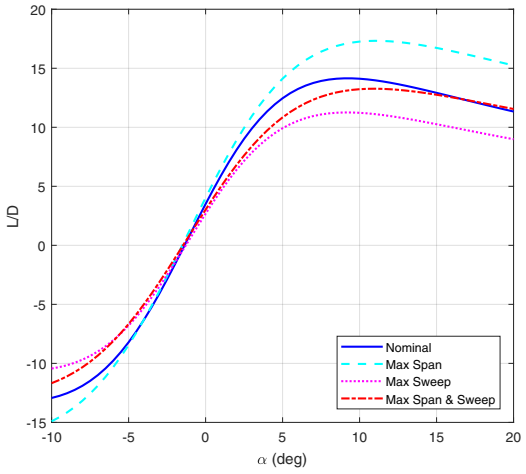

Fig. 4. Lift-to-drag ratio curves

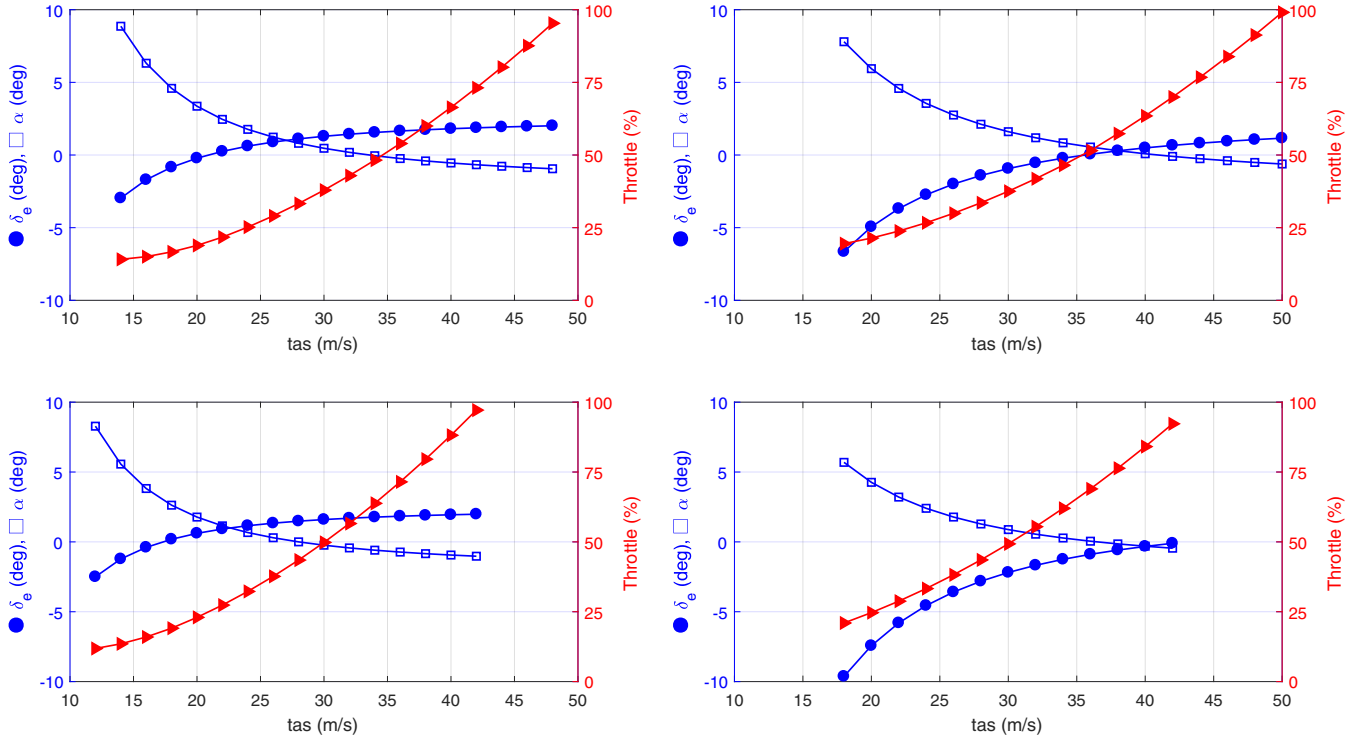

Fig. 5. Trim maps, nominal (upper left), max span (lower left), max sweep (upper right), max span & sweep (lower right)

III. Input-Output Linearization

The longitudinal-axis equations of motion of the morphing UAV can be written as a special case of multi-input multi-output (MIMO) nonlinear systems of the form as

$$\dot{x} = f(x) + \sum_{k=1}^{m} g_k(x) u_k \tag{11}$$

$$y_i = h_i(x), \quad i = 1, \ldots, m \tag{12}$$

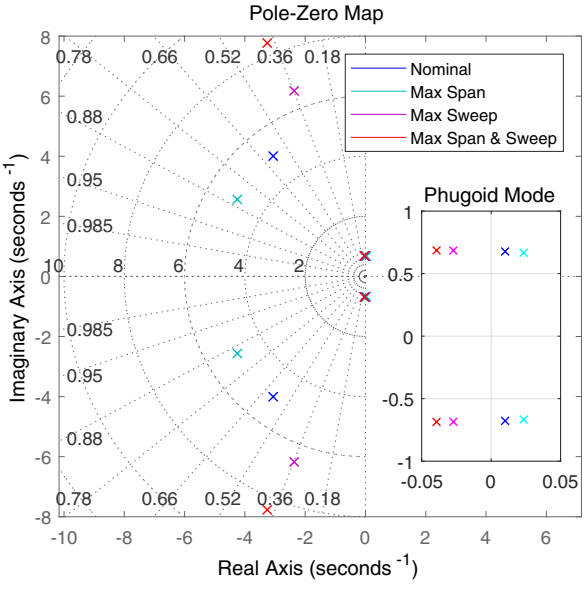

Fig. 6. Open-loop poles

where $x = [V\ \gamma\ \alpha\ \sigma\ h]^T$, $u = [\sigma_c\ \delta_e]^T$, and $y = [V\ h]^T$. Note that the number of control inputs and controlled outputs are equal in this case ($m = 2$). Assuming that $\frac{\partial C_L}{\partial \delta_e}$ and $\frac{\partial C_D}{\partial \delta_e}$ are negligibly small, the minimum orders of the derivatives of y_i for which the coefficient g_k of at least one u_k is strictly nonzero are 3 for V and 4 for h. This means that the relative degree of the system is equal to the order of the system, and therefore the considered nonlinear system is input-output (IO) linearizable. The IO linearized system can be obtained by repeatedly differentiating the outputs V and h as follows [5].

$$\dot{V} = f_1 \tag{13}$$

$$\ddot{V} = \frac{\omega_1 \dot{x}}{m} \tag{14}$$

$$\dddot{V} = \frac{\omega_1 \ddot{x} + \dot{x}^T \Omega_2 \dot{x}}{m} \tag{15}$$

$$\dot{h} = V \sin\gamma \tag{16}$$

$$\ddot{h} = \dot{V} \sin\gamma + V\dot{\gamma}\cos\gamma \tag{17}$$

$$\dddot{h} = \ddot{V}\sin\gamma + 2\dot{V}\dot{\gamma}\cos\gamma - V\dot{\gamma}^2\sin\gamma + V\ddot{\gamma}\cos\gamma \tag{18}$$

$$h^{(4)} = \dddot{V}\sin\gamma + 3\ddot{V}\dot{\gamma}\cos\gamma - 3\dot{V}\dot{\gamma}^2\sin\gamma + 3\dot{V}\ddot{\gamma}\cos\gamma - 3V\dot{\gamma}\ddot{\gamma}\sin\gamma - V\dot{\gamma}^3\cos\gamma + V\dddot{\gamma}\cos\gamma \tag{19}$$

where

$$\dot{\gamma} = f_2 \tag{20}$$

$$\ddot{\gamma} = \pi_1 \dot{x} \tag{21}$$

$$\dddot{\gamma} = \pi_1 \ddot{x} + \dot{x}^T \Pi_2 \dot{x} \tag{22}$$

The terms $\omega_1, \omega_2, \pi_1$, and Π_2 are listed in Appendix.

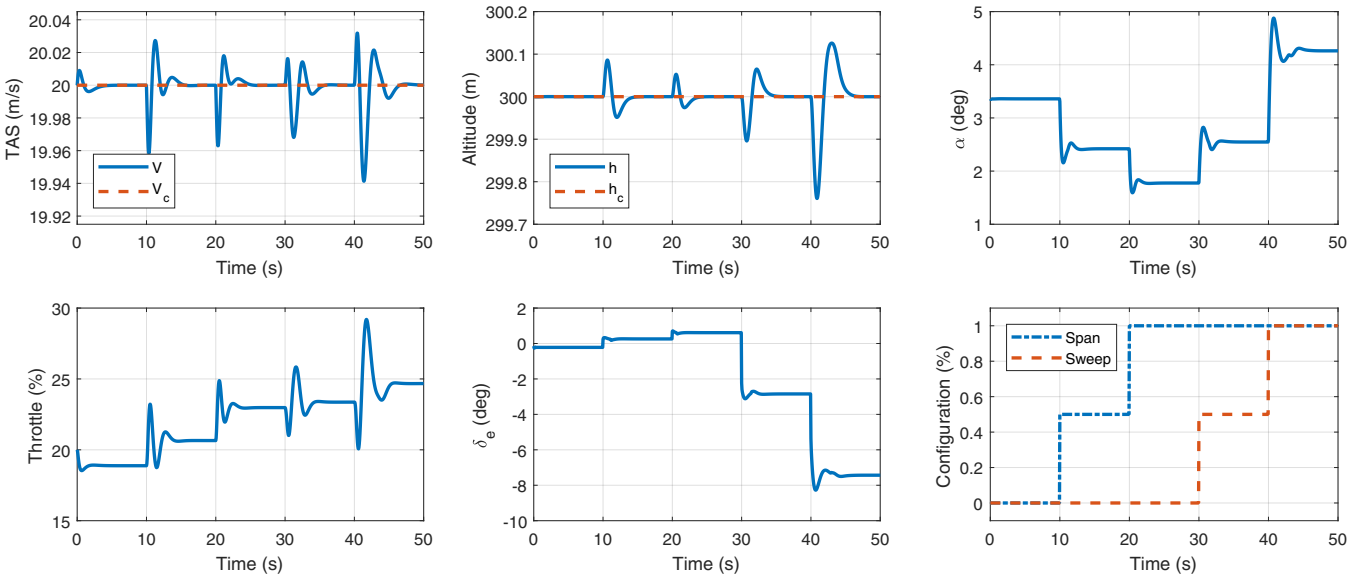

Fig. 7. Regulation results

The second derivatives of α and σ can be expressed as

$$\ddot{\alpha} = \ddot{\alpha}_0 + \left(\frac{\rho V^2 S\bar{c} C_{M_{\delta_e}}}{2I_y}\right)\delta_e \tag{23}$$

$$\ddot{\sigma} = \ddot{\sigma}_0 + \omega_n^2 \sigma_c \tag{24}$$

where

$$\ddot{\alpha}_0 = \frac{\frac{1}{2}\rho V^2 S\bar{c}(C_{M_0} + C_{M_\alpha}\alpha)}{I_y} - \ddot{\gamma} \tag{25}$$

$$\ddot{\sigma}_0 = -2\zeta\omega_n\dot{\sigma} - \omega_n^2\sigma \tag{26}$$

Note that C_M can be expressed in terms of stability and control derivatives as in (23) and (25), and they are virtually independent of the angle of attack and the configuration. The output dynamics can be written as

$$\dddot{V} = f_V + b_{11}\sigma_c + b_{12}\delta_e \tag{27}$$

$$h^{(4)} = f_h + b_{21}\sigma_c + b_{22}\delta_e \tag{28}$$

where

$$f_V = \frac{\omega_1\ddot{x}_0 + \dot{x}^T\Omega_2\dot{x}}{m} \tag{29}$$

$$\begin{aligned} f_h = &\left(\frac{\omega_1\ddot{x}_0 + \dot{x}^T\Omega_2\dot{x}}{m}\right)\sin\gamma + 3\ddot{V}\dot{\gamma}\cos\gamma \\ &- 3\dot{V}\dot{\gamma}^2\sin\gamma + 3\dot{V}\ddot{\gamma}\cos\gamma - 3V\dot{\gamma}\ddot{\gamma}\sin\gamma \\ &- V\dot{\gamma}^3\cos\gamma + V\cos\gamma(\pi_1\ddot{x}_0 + \dot{x}^T\Pi_2\dot{x}) \end{aligned} \tag{30}$$

$$b_{11} = \frac{T_{max}\omega_n^2\cos\alpha}{m} \tag{31}$$

$$b_{12} = -\left(\frac{\rho V^2 S\bar{c} C_{M_{\delta_e}}}{2mI_y}\right)\left[T\sin\alpha + \frac{1}{2}\rho V^2 S\frac{\partial C_D}{\partial\alpha}\right] \tag{32}$$

$$b_{21} = \frac{T_{max}\omega_n^2\sin(\alpha+\gamma)}{m} \tag{33}$$

$$\begin{aligned} b_{22} = &\left(\frac{\rho V^2 S\bar{c} C_{M_{\delta_e}}}{2mI_y}\right)\left[T\cos(\alpha+\gamma)\right. \\ &\left. + \frac{1}{2}\rho V^2 S\left(\frac{\partial C_L}{\partial\alpha}\cos\gamma - \frac{\partial C_D}{\partial\alpha}\sin\gamma\right)\right] \end{aligned} \tag{34}$$

where

$$\ddot{x}_0 = [\ddot{V}\ \ddot{\gamma}\ \ddot{\alpha}_0\ \ddot{\sigma}_0\ \ddot{h}]^T \tag{35}$$

IV. Sliding Mode Controller Design

In this study, two sliding variables are defined as follows,

$$s_1 = \left(\frac{d}{dt} + \lambda_1\right)^3 \int_0^t e_1(\tau)d\tau, \quad e_1 = V - V_d \tag{36}$$

$$s_2 = \left(\frac{d}{dt} + \lambda_2\right)^4 \int_0^t e_2(\tau)d\tau, \quad e_2 = h - h_d \tag{37}$$

where positive constants λ_1 and λ_2 determine the bandwidth of the error dynamics. Differentiating s_1 and s_2, we have

$$\dot{s} = \upsilon + Bu \tag{38}$$

where

$$s = \begin{bmatrix} s_1 \\ s_2 \end{bmatrix}, \quad \upsilon = \begin{bmatrix} \upsilon_1 \\ \upsilon_2 \end{bmatrix}, \quad B = \begin{bmatrix} b_{11} & b_{12} \\ b_{21} & b_{22} \end{bmatrix} \tag{39}$$

$$\upsilon_1 = -\dddot{V}_d + f_V + 3\lambda_1\ddot{e}_1 + 3\lambda_1^2\dot{e} + \lambda_1^3 e_1 \tag{40}$$

$$\upsilon_2 = -h_d^{(4)} + f_h + 4\lambda_2\dddot{e}_2 + 6\lambda_2^2\ddot{e}_2 + 4\lambda_2^3\dot{e}_2 + \lambda_2^4 e_2 \tag{41}$$

Let us consider a control law of the form below.

$$u = B^{-1}\begin{bmatrix} -\upsilon_1 - k_1\mathrm{sgn}(s_1) \\ -\upsilon_2 - k_2\mathrm{sgn}(s_2) \end{bmatrix} \tag{42}$$

Using (36)-(42), we have

$$\frac{d}{dt}\left(\frac{1}{2}s_i^2\right) = -k_i|s_i|, \quad i = 1,2 \tag{43}$$

where k_1 and k_2 are positive constants which can be adjusted to change the reaching time to the sliding surfaces. To avoid

chattering phenomena, saturation functions with boundary layers of width Φ_1 and Φ_2 are used instead of the signum function as

$$u = B^{-1}\begin{bmatrix} -\upsilon_1 - k_1 \text{sat}(\frac{s_1}{\Phi_1}) \\ -\upsilon_2 - k_2 \text{sat}(\frac{s_2}{\Phi_2}) \end{bmatrix} \tag{44}$$

V. Numerical Simulation

Numerical simulation is performed to demonstrate the effectiveness of the proposed scheme. Three different cases are considered: a regulation case (Fig. 7), a TAS 5m/s step command tracking case (Fig. 8), and an altitude 20m step command tracking case (Fig. 9). Selection of the control gains for each case are shown in Table I.

TABLE I
Control parameters

-	k_1	k_2	Φ_1	Φ_2	λ_1	λ_2
Regulation	10	10	1	1	2	3
Tracking	50	50	2	2	1/3	1/2

In the regulation case, two morphing parameters are successively changed from 0 to 1 (Fig. 7). Note that the sliding mode controller tightly maintains the cruise speed and altitude even in the presence of large-scale configuration changes during the flight. Tracking simulation results (Figs. 8 and 9) show that the transient responses can be changed in different morphing configurations. It can be stated that the results can provide useful information for the design of an active morphing-aided control system where the configuration is automatically adjusted to improve the transient responses.

VI. Conclusions

In this study, a longitudinal dynamic model of a novel span and sweep-varying morphing unmanned aerial vehicle was developed. A sliding mode control technique was applied to the airspeed and altitude control problem. Numerical simulation is performed to demonstrate the effectiveness of the proposed scheme.

APPENDIX

Expressions of $\omega_1, \omega_2, \pi_1$, and Π_2 in (13)-(22) are as follows [6].

$$\omega_1 = \frac{\partial f_1}{\partial x} = \begin{bmatrix} -\rho V S C_D \\ -g\cos\gamma \\ -T\sin\alpha - \frac{1}{2}\rho V^2 S \frac{\partial C_D}{\partial \alpha} \\ T_{max}\cos\alpha \\ -\frac{1}{2}\frac{\partial \rho}{\partial h} V^2 S C_D \end{bmatrix}^T$$

$$\pi_1 = \frac{\partial f_2}{\partial x} = \begin{bmatrix} \frac{\rho S C_L}{2m} - \frac{T\sin\alpha}{mV^2} \\ \frac{g\sin\gamma}{V} \\ \frac{\rho V S C_{L_\alpha}}{2m} + \frac{T\cos\alpha}{mV} \\ \frac{T_{max}\sin\alpha}{mV} \\ \frac{V S C_L}{2m}\frac{\partial \rho}{\partial h} \end{bmatrix}^T$$

$$\Omega_2 = \frac{\partial \omega_1^T}{\partial x} = \begin{bmatrix} \omega_{21} & \omega_{22} & \omega_{23} & \omega_{24} & \omega_{25} \end{bmatrix}$$

$$\Pi_2 = \frac{\partial \pi_1^T}{\partial x} = \begin{bmatrix} \pi_{21} & \pi_{22} & \pi_{23} & \pi_{24} & \pi_{25} \end{bmatrix}$$

where

$$\omega_{21} = \begin{bmatrix} -\rho S C_D \\ 0 \\ -\rho V S \frac{\partial C_D}{\partial \alpha} \\ 0 \\ -\frac{\partial \rho}{\partial h} V S C_D \end{bmatrix} \qquad \omega_{22} = \begin{bmatrix} 0 \\ g\sin\gamma \\ 0 \\ 0 \\ 0 \end{bmatrix}$$

$$\omega_{23} = \begin{bmatrix} -\rho V S \frac{\partial C_D}{\partial \alpha} \\ 0 \\ -T\cos\alpha - \rho V^2 S C_{D_{\alpha^2}} \\ -T_{max}\sin\alpha \\ -\frac{1}{2}\frac{\partial \rho}{\partial h} V^2 S \frac{\partial C_D}{\partial \alpha} \end{bmatrix} \qquad \omega_{24} = \begin{bmatrix} 0 \\ 0 \\ -T_{max}\sin\alpha \\ 0 \\ 0 \end{bmatrix}$$

$$\omega_{25} = \begin{bmatrix} -\frac{\partial \rho}{\partial h} V S C_D \\ 0 \\ -\frac{1}{2}\frac{\partial \rho}{\partial h} V^2 S \frac{\partial C_D}{\partial \alpha} \\ 0 \\ -\frac{1}{2}\frac{\partial^2 \rho}{\partial h^2} V^2 S C_D \end{bmatrix} \qquad \pi_{21} = \begin{bmatrix} \frac{2T\sin\alpha}{mV^3} \\ 0 \\ \frac{\rho S C_{L_\alpha}}{2m} - \frac{T\cos\alpha}{mV^2} \\ -\frac{T_{max}\sin\alpha}{mV^2} \\ \frac{\partial \rho}{\partial h}\frac{S C_L}{2m} \end{bmatrix}$$

$$\pi_{22} = \begin{bmatrix} -\frac{g\sin\gamma}{V^2} \\ \frac{g\cos\gamma}{V} \\ 0 \\ 0 \\ 0 \end{bmatrix} \qquad \pi_{23} = \begin{bmatrix} \frac{\rho S C_{L_\alpha}}{2m} - \frac{T\cos\alpha}{mV^2} \\ 0 \\ -\frac{T\sin\alpha}{mV} \\ \frac{T_{max}\cos\alpha}{mV} \\ \frac{\partial \rho}{\partial h}\frac{V S C_{L_\alpha}}{2m} \end{bmatrix}$$

$$\pi_{24} = \begin{bmatrix} -\frac{T_{max}\sin\alpha}{mV^2} \\ 0 \\ \frac{T_{max}\cos\alpha}{mV} \\ 0 \\ 0 \end{bmatrix} \qquad \pi_{25} = \begin{bmatrix} \frac{1}{2m}\frac{\partial \rho}{\partial h} S C_L \\ 0 \\ \frac{1}{2m}\frac{\partial \rho}{\partial h} V S C_{L_\alpha} \\ 0 \\ \frac{1}{2m}\frac{\partial^2 \rho}{\partial h^2} V S C_L \end{bmatrix}$$

References

[1] S. Barbarino, O. Bilgen, R. M. Ajaj, M. I. Friswell, and D. J. Inman, A Review of Morphing Aircraft, *Journal of Intelligent Material Systems and Structures*, vol. 22, no. 9, pp. 823-877, 2011.

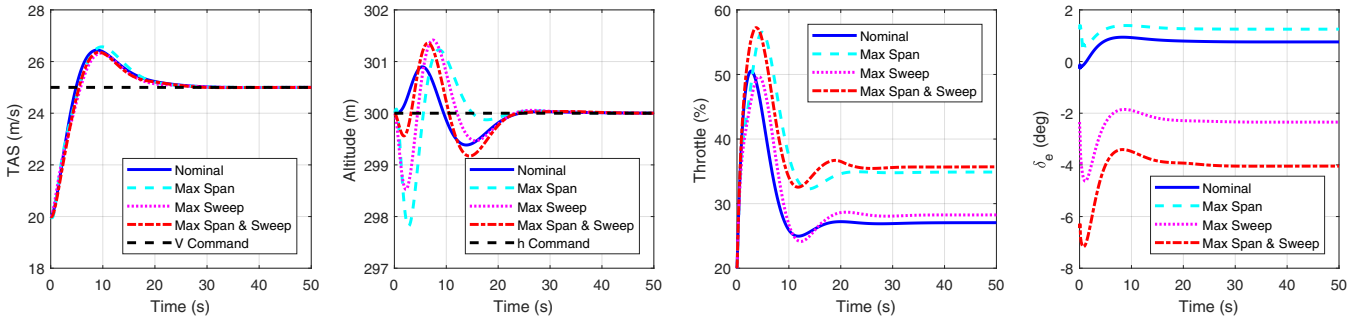

Fig. 8. TAS step command tracking results

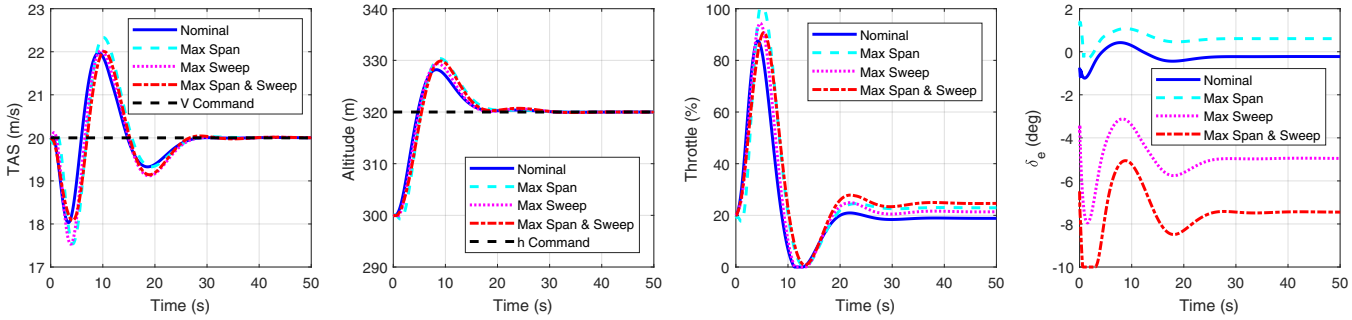

Fig. 9. Altitude step command tracking results

[2] J. Valasek, *Morphing Aerospace Vehicles and Structures*, Chichester, UK: John Wiley & Sons, Ltd., 2012.

[3] The XFLR5 website: http://www.xflr5.com/xflr5.htm

[4] B. L. Stevens, F. L. Lewis, and E. N. Johnson, *Aircraft Control and Simulation*, 3rd ed. Hoboken, NJ: John Wiley & Sons, Inc., pp. 111-116, 2016.

[5] H. Xu, M. D. Mirmirani, and P. A. Ioannou, Adaptive Sliding Mode Control Design for a Hypersonic Flight Vehicle, *Journal of Guidance, Control, and Dynamics*, vol. 27, no. 5, pp. 829-838, 2004.

[6] Q. Wang and R. F. Stengel, Robust Nonlinear Control of a Hypersonic Aircraft, *Journal of Guidance, Control, and Dynamics*, vol. 23, no. 4, pp. 577-585, 2000.